Journal of Materials Chemistry B

# Multi-responsive graft copolymer micelles comprising acetal and disulfide linkages for stimuli-triggered drug delivery



| | |
|---|---|
| Journal: | *Journal of Materials Chemistry B* |
| Manuscript ID: | TB-ART-03-2015-000473 |
| Article Type: | Paper |
| Date Submitted by the Author: | 14-Mar-2015 |





| | |
|---|---|
| Complete List of Authors: | Zhao, Youliang; Soochow University, College of Chemistry, Chemical Engineering and Materials Science<br>Liu, Huanhuan; Soochow University,<br>Li, Cangxia; Soochow University,<br>Tang, Dandan; Soochow University,<br>An, Xiaonan; Soochow University,<br>Guo, Yanfei; Soochow University, |

Journal Name RSCPublishing

# Multi-responsive graft copolymer micelles comprising acetal and disulfide linkages for stimuli-triggered drug delivery†

Cite this: DOI: 10.1039/x0xx00000x

Received 00th January 2012,
Accepted 00th January 2012

DOI: 10.1039/x0xx00000x

www.rsc.org/

Huanhuan Liu, Cangxia Li, Dandan Tang, Xiaonan An, Yanfei Guo and Youliang Zhao*

Thermo, pH and reduction triggered drug delivery vehicles based on dual-cleavable polymeric micelles were investigated. A comblike copolymer (G3) comprising one disulfide linkage and PEG, PCL and acetal-bridged PCL-*b*-PNIPAM grafts was controllably synthesized by successive RAFT copolymerization, ring-opening polymerization and adductive reaction. G3 was liable to self-assemble into spherical micelles at 25 $^{o}$C and toroidal micelles at 37 $^{o}$C, and the aggregates formed at 37 $^{o}$C could be further converted into multicompartment micelles (pH 5.3), spherical micelles (DTT) and hyperbranched or necklace-like cylinders (pH 5.3 + DTT) upon external stimuli due to stimuli-triggered topological transformation and reaggregation of copolymer aggregates. Upon external stimuli, the doxorubicin (DOX) loaded G3 and G3/$\beta$-CD (co)aggregates could exhibit accelerated drug release kinetics. The apparent release rates varied in the range 0.072-0.403 $h^{-1}$ (for G3 aggregates) and 0.142-0.458 $h^{-1}$ (for G3/$\beta$-CD coaggregates), revealing the drug release system bearing host-guest interactions could further extend the ranges of release rate and cumulative release. Although $\beta$-CD and G3 micelles lacked notable cytotoxicity, the cytotoxicity of DOX-loaded (co)aggregates to 4T1 cells was higher than free DOX. CLSM images revealed that DOX-loaded copolymer aggregates may enter cells via endocytosis in a manner of nanocomplex. Our study can not only extend the potential of stimuli-cleavable copolymers toward biomedical applications but enrich the family of multi-responsive copolymer aggregates.

## Introduction

Stimuli-responsive polymeric aggregates have attracted wide attention due to their versatile applications involving the enhanced selectivity and efficiency of drug delivery to targeting sites.[1–15] Functional aggregates formed from dually and multiply stimuli-sensitive copolymers have been used for smart drug release systems (SDRS), in which various internal and external stimuli have been widely applied to induce the dissociation or morphology transition of copolymer aggregates and accelerate the release process.[1–37] Among various triggers, thermo-stimulus is popular due to its easy control and practical advantages, whilst pH and reduction stimuli are applied to improve intracellular anticancer drug delivery.[11–35] The pH can vary from about 7.4 (physiological), 6.8 (extracellular in tumor tissues) to 4.0-6.5 (intracellular endo/lysosomal), and the pH gradient between cancer and normal tissues allows for specific targeting and controlled release of drugs at the tumor site. Meanwhile, the concentration of glutathione (GSH) in biological systems ranges from 2–20 μM (in the extracellular matrix) to 2–10 mM (in the intracellular compartments) and further enhances in the malignant tumor, and the large redox potential renders GSH an effective cellular trigger to cleave disulfide linkages, leading to faster drug release within the cells in redox-sensitive systems. A classical model of drug release involves a diffusion-controlled mechanism which requires overcoming hydrophobic interactions between drugs and micellar core-forming polymers, and the release process is uncontrolled and slow.[38] A promising approach to address this limitation is to incorporate cleavable linkages in amphiphilic copolymers, and stimuli-triggered degradation and reassembly of aggregates can efficiently enhance the release process. The introduction of labile linkages can not only enrich the types of copolymer aggregates but generate intriguing properties for versatile applications. However, copolymers with dual- and multi-labile linkages to bridge polymer segments have been scarcely reported thus far.[20–25] It is timely to generate such copolymers and extend their potential in bioscience and smart materials.

Among host-guest systems, cyclodextrins ($\alpha$, $\beta$, and $\gamma$-CD) with torus-like structure and hydrophobic cavity are a series of natural cyclic oligosaccharides consisting of 6, 7, or 8 D(+)-glucose units,[39] and they can dissolve in water and have low toxicity in animals and humans.[40] These macrocyclic hosts are readily functionalized and commercially available, and their hydrophobic cavity can be threaded by linear polymer such as PEG and PCL to form the inclusion complexes. Owing to significant changes in physical, chemical and biological properties via host-guest interactions, cyclodextrins are promising candidates for gene and drug delivery.[40–60] Besides CD-based macromolecular architectures with

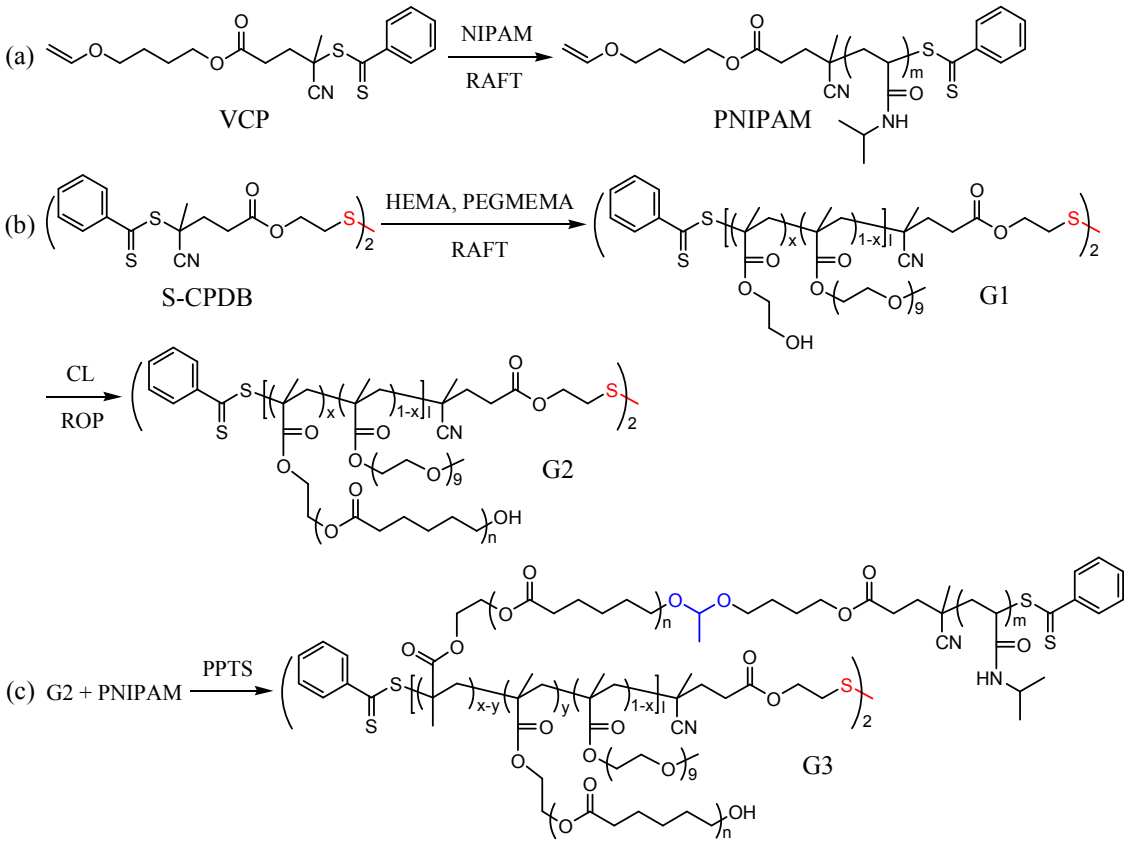


**Scheme 1** Synthetic routes to vinyloxy-terminated PNIPAM (a), disulfide-linked poly(HEMA-*co*-PEGMEMA) (G1) and comblike poly(PEG-*co*-PCL) (G2), and dual-cleavable poly(PEG-*co*-PCL)-*graft*-PNIPAM (G3).

covalent linkages, increasing attention has been paid to construct functional inclusion complexes,[46–50] coaggregates,[51–56] nano- and microgels[57–60] for targeted delivery via supramolecular self-assembly. Among them, the CD-based supramolecular systems allow tunable and competitive host-guest and hydrogen-bonding interactions in some cases,[51] which further enhance the functions and parameters during release process.[40–45] The best advantages of host-guest assembly lie in flexibility and controllability, which lack tedious chemical synthesis and allow systematic optimization via changing the functional tags responding to a request. To the best of our knowledge, multi-responsive coaggregates comprising CD and dual-cleavable copolymer toward biomedical applications have not been reported, and it is urgent to fabricate such host-guest vehicles for SDRS.

As an important member of complex macromolecular architectures, graft polymer has attracted much attention due to its unique properties and potential applications in many fields. Depending on molecular parameters, graft polymers can be subjected to microphase separation and form rich nanostructures and morphologies, and their physicochemical properties such as mechanical properties, viscosity and glass transition temperature are usually different from their linear counterparts.[61–72] Some approaches such as “grafting onto”, “grafting through” and “grafting from” processes have been utilized for the controlled synthesis, and numerous graft polymers with variable grafting density and versatile chemical compositions have been successfully achieved.[61–72] Meanwhile, the latest advances in controlled polymerization and linkage reaction further extend the ranges of functionalities and applications of graft polymers. Owing to the crucial roles of structural complexity and special function in advanced biomedical materials, it is of great importance to further explore facile approaches to construction of novel graft polymers. More recently, two types of graft copolymers with biocompatible poly(ethylene glycol) (PEG) and biodegradable poly(ε-caprolactone) (PCL) grafts and disulfide and acetal linkages were synthesized and self-assembled for loading and release of doxorubicin (DOX), and the results revealed the drug release kinetics was strongly dependent on external stimuli, macromolecular architecture and location of acetal linkages.[24,25] Considering that PEG and PCL grafts lack stimulus responsiveness, it is worth introducing stimuli-sensitive segments into functional graft copolymers to construct multi-responsive systems toward biomedical applications.

This study aimed at synthesis and properties of a dual-cleavable graft copolymer bearing PEG, PCL and PCL-*b*-PNIPAM side chains, in which poly(*N*-isopropylacrylamide) (PNIPAM) was chosen as a model stimuli-responsive segment. The disulfide moiety was derived from the original chain transfer agent S-CPDB,[70] and acetal-bridged PCL-*b*-PNIPAM grafts were generated by adductive reaction between hydroxyl-terminated PCL and vinyloxy-functionalized PNIPAM (Scheme 1). The target copolymer poly(PEG-*co*-PCL)-*graft*-PNIPAM (G3) was synthesized by successive reactions involving reversible addition–fragmentation

 

chain transfer (RAFT) process,[73] ring-opening polymerization (ROP) and hydroxyl-vinyloxy adductive reaction. On this basis, drug loading and stimuli-triggered release from copolymer aggregates formed from G3 and G3/*β*-CD mixture were investigated. This study described facile synthesis and properties of the first example of dual-cleavable multi-responsive graft copolymers, and the general method allowed for introduction of a wide range of stimuli-sensitive polymer segments with tunable graft numbers and versatile compositions. Moreover, G3 aggregates and G3/*β*-CD coaggregates exhibited adjustable drug release kinetics upon acid, reduction and thermo stimuli, revealing their great potential in multi-triggered SDRS.

## Experimental section

### Materials

All solvents, monomers, and other chemicals were purchased from Sigma-Aldrich unless otherwise stated. Poly(ethylene glycol) methyl ether methacrylate (PEGMEMA, $M_n \approx 475$, 99%) and 2-hydroxyethyl methacrylate (HEMA, 99%) were passed through a basic alumina column to remove the inhibitor. *ε*-Caprolactone (CL, 99%) and bis(2-hydroxyethyl) disulfide (Alfa Aesar, 90%) were distilled under reduced pressure. *N*-Isopropylacrylamide (NIPAM, 97%) was recrystallized twice from mixtures of hexane and toluene, and 2,2′-azobis(isobutyronitrile) (AIBN) was recrystallized twice from ethanol. Dioxane and toluene were distilled over sodium and benzophenone, and *N*,*N*-dimethylformamide (DMF) distilled under reduced pressure after drying over $MgSO_4$. Disulfide-linked RAFT agent S-CPDB[70] and 4-cyanopentanoic acid dithiobenzoate (4-CPDB)[74] were synthesized and purified according to literature procedures. *N*,*N*′-Dicyclohexylcarbodiimide (DCC) and 4-dimethylamino pyridine (DMAP) were purchased from Sinopharm Chemical Reagent Co., Ltd. and used as received. 4-Hydroxybutyl vinyl ether (99%, J&K Scientific Ltd), stannous octoate ($Sn(Oct)_2$, 97%), DL-dithiothreitol (DTT, 99%, Merck), and doxorubicin hydrochloride (DOX HCl, > 99%, Zhejiang Hisun Pharmaceutical Co, Ltd.) were used as received.

### Synthesis of VCP

To a round flask were added 4-hydroxybutyl vinyl ether (1.16 g, 10.0 mmol), 4-CPDB (2.79 g, 10.0 mmol), DMAP (0.122 g, 1.0 mmol) and dry dichloromethane (100 mL), and the solution was cooled with ice-water bath. Under nitrogen, 20 mL of DCM solution with 2.50 g (12.1 mmol) of DCC was slowly added to the above solution in 30 min. The contents were further stirred at ambient temperature for 20 h. After filtration, the filtrate was partitioned between water and dichloromethane. The aqueous layer was extracted twice with DCM, and then the combined extracts were dried over $MgSO_4$ overnight. The crude product was purified by flash column chromatography eluting with hexane / ethyl acetate (30:1, v/v), and 3.20 g (84.8% yield) of 4-(vinyloxy)butyl 4-cyano-4-(phenylcarbonothioylthio)pentanoate (VCP) was obtained.

VCP: $^1$H NMR ($CDCl_3$): $\delta$ 7.92 (d, *J* 7.2, 2H, Ph*H*), 7.57 (t, *J* 7.6, 1H, Ph*H*), 7.40 (t, *J* 8.0, 2H, Ph*H*), 6.47 (m, 1H, OC*H*=$CH_2$), 4.19, 4.00 (each dd, 2H, OCH=C$H_2$), 4.15 (t, *J* 6.4, 2H, COOC$H_2$), 3.71 (t, *J* 6.4, 2H, C$H_2$O), 2.3-2.8 (m, 4H, COC$H_2$C$H_2$), 1.94 (s, 3H, C$H_3$), 1.75 (m, 4H, C$H_2$C$H_2$CH$_2$O). $^{13}$C NMR ($CDCl_3$): $\delta$ 222.2 (*C*=S), 171.4 (*C*=O), 151.6 (*C*H=$CH_2$), 144.3, 133.0, 128.5, 126.5 (Ph*C*), 118.4 (*C*N), 86.4 (CH=*C*$H_2$), 67.1, 64.6 (*C*$H_2$O), 45.6 (*C*-CN), 33.3, 29.7, 25.5, 25.2 (*C*$H_2$), 24.0 (*C*$H_3$). FT-IR (KBr): 2932, 2856, 1734, 1637, 1579, 1563, 1446, 1385, 1344, 1318, 1292, 1186, 1129, 1112, 1085, 1048, 1000, 902, 869, 817, 764, 741, 689 cm$^{-1}$.

### Synthesis of vinyloxy-terminated PNIPAM

NIPAM (1.19 g, 10.5 mmol), VCP (56.6 mg, 0.15 mmol) and AIBN (12.3 mg, 0.075 mmol) were added to a Schlenk tube, and dioxane was added until the total volume was 4.2 mL. The contents were flushed with nitrogen for 20 min, and followed by polymerization at 70 °C for 18 h. The solution was cooled down and precipitated into cold diethyl ether thrice, and 1.53 g (81.0% conversion) of vinyloxy-terminated PNIPAM was obtained after vacuum drying. Apparent molecular weight and polydispersity (PDI) estimated by GPC were $M_{n,GPC}$ = 6580 and PDI = 1.13, and the degree of polymerization (DP) and number-average molecular weight were determined to be DP = 56.4, and $M_{n,NMR}$ = 6750 by $^1$H NMR analysis.

PNIPAM: $^1$H NMR ($CDCl_3$): $\delta$ 7.96, 7.56, 7.39 (m, Ph*H*), 6.0-7.2 (m, OC*H*=$CH_2$ and N*H* of PNIPAM), 4.5-4.8 (m, C*H*S), 3.9-4.2 (m, OCH=C$H_2$, COOC$H_2$, and C*H* of PNIPAM), 3.66 (m, C$H_2$O), 0.6-2.5 (other C*H*, C$H_2$ and C$H_3$ originating from CTA and PNIPAM). FT-IR (KBr): 3072, 2973, 2935, 2876, 1650, 1544, 1459, 1386, 1367, 1327, 1173, 1130, 1046, 990, 928, 881, 839, 802, 764, 690 cm$^{-1}$.

### Synthesis of poly(HEMA-*co*-PEGMEMA)

HEMA (0.52 g, 4.0 mmol), PEGMEMA (1.90 g, 4.0 mmol), S-CPDB (0.135 g, 0.20 mmol) and AIBN (13.2 mg, 0.08 mmol) were added to a Schlenk tube, and DMF was added until the total volume was 4.0 mL. The contents were flushed with nitrogen for 20 min and subjected to polymerization at 60 °C for 8 h. The polymer solution was concentrated and precipitated into cold diethyl ether thrice, and 2.32 g (90.3% conversion) of poly(HEMA-*co*-PEGMEMA) (G1) was obtained. Apparent molecular weight and polydispersity (PDI) estimated by GPC were $M_{n,GPC}$ = 14300 and PDI = 1.11, and DP and $M_n$ values were determined to be $DP_{HEMA}$ = 18.0, $DP_{PEGMEMA}$ = 18.2, and $M_{n,NMR}$ = 11700 by $^1$H NMR analysis.

G1: $^1$H NMR (DMSO-$d_6$): $\delta$ 7.82, 7.64, 7.47 (m, Ph*H*), 4.77 (m, CH$_2$O*H*), 4.26 (m, COOC$H_2$CH$_2$S), 4.01 (m, COOC$H_2$ of PEGMEMA unit), 3.89 (m, COOC$H_2$ of HEMA unit), 3.3-3.7 (m, C$H_2$OH of HEMA unit, and C$H_2$O of PEGMEMA unit), 3.24 (s, C$H_3$O of PEG), 2.97 (m, C$H_2$S), 0.5-2.2 (m, other C$H_2$ and C$H_3$ originating from CTA and monomer units). FT-IR (KBr): 3414, 2878, 1728, 1639, 1454, 1386, 1353, 1276, 1249, 1109, 1033, 951, 850, 748, 693 cm$^{-1}$.

### Synthesis of poly(PEG-*co*-PCL)

To a Schlenk tube were added G1 (0.65 g, 1.0 mmol of OH), CL (1.71 g, 15.0 mmol), and $Sn(Oct)_2$ (41 mg, 0.10 mmol) under nitrogen, and then toluene was added until the total volume was 7.5 mL. After three freeze-vacuum-thaw cycles, the contents were polymerized at 90 °C for 24 h, and 2.26 g (94.2% conversion) of poly(PEG-*co*-PCL) comblike copolymer (G2) was isolated by precipitation into cold methanol. The molecular weight and polydispersity determined by GPC-MALLS were $M_{n,LS}$ = 39200 and PDI = 1.13. NMR analysis: $DP_{PCL}$ = 14.4, $M_{n,NMR}$ = 41300.

G2: $^1$H NMR (DMSO-$d_6$): $\delta$ 7.4-7.9 (m, Ph*H*), 4.1-4.5 (m, OC$H_2$C$H_2$O and OC$H_2$CH$_2$S), 3.99 (m, C$H_2$O of PCL and COOC$H_2$ of PEGMEMA unit), 3.51 (m, C$H_2$O of PEGMEMA unit, and terminal C$H_2$OH of PCL), 3.24 (s, C$H_3$O), 2.97 (m,

**Table 1** Molecular parameters and DSC results of vinyloxy-terminated PNIPAM, disulfide-linked poly(HEMA-*co*-PEGMEMA) (G1), comblike poly(PEG-*co*-PCL) (G2), and dually cleavable poly(PEG-*co*-PCL)-*graft*-PNIPAM (G3)[a]

| run | sample | $M_n$[b] | PDI[b] | $M_{n,NMR}$[c] | $DP_1$[d] | $DP_2$[d] | $DP_{PCL}$[d] | $m_{PNIPAM}$[e] | $T_g$ (°C)[f] | $T_m$ (°C)[f] |
|---|---|---|---|---|---|---|---|---|---|---|
| 1 | PNIPAM | 6580 | 1.13 | 6750 | — | — | — | — | 116.0 | — |
| 2 | G1 | 14300 | 1.11 | 11700 | 18.0 | 18.2 | 0 | 0 | -46.3, -12.2 | — |
| 3 | G2 | 39200 | 1.13 | 41300 | 18.0 | 18.2 | 14.4 | 0 | -71.6, -51.7 | 21.4, 29.0 |
| 4 | G3 | 78500 | 1.18 | 77600 | 18.0 | 18.2 | 14.4 | 5.7 | -63.7, -15.1, 112.5 | — |

[a] Reaction conditions: $[NIPAM]_0:[VCP]_0:[AIBN]_0$ = 70:1:0.2, $[NIPAM]_0$ = 2.5 mol $L^{-1}$, in dioxane at 70 °C for 18 h (run 1); $[HEMA]_0:[PEGMEMA]_0:[S\text{-}CPDB]_0:[AIBN]_0$ = 20:20:1:0.4, $[HEMA]_0$ = 1.5 mol $L^{-1}$, in DMF at 60 °C for 8 h (run 2); $[CL]_0:[OH]_0:[Sn(Oct)_2]_0$ = 15:1:0.1, $[CL]_0$ = 2.0 mol $L^{-1}$, in toluene at 90 °C for 24 h (run 3); $[OH]_0:[PNIPAM]_0:[PPTS]_0$ = 5:3:1, $W_{polymer}:V_{DMF}$ = 0.20 g $mL^{-1}$, in DMF at 40 °C for 36 h. [b] Molecular weight and polydispersity estimated by GPC ($M_{n,GPC}$, for PNIPAM and G1) or determined by GPC-MALLS ($M_{n,LS}$, for other samples). [c] Molecular weight ($M_{n,NMR}$) determined by $^1$H NMR analysis. [d] Degree of polymerization of HEMA ($DP_1$), PEGMEMA ($DP_2$) and PCL ($DP_{PCL}$) determined by $^1$H NMR analysis. [e] Number of grafted PNIPAM per copolymer determined by $^1$H NMR analysis. [f] Glass transition temperature ($T_g$) and maximal melting temperature ($T_m$) determined by DSC.

C*H*$_2$S), 0.5-2.4 (m, other C*H*$_2$ and C*H*$_3$ originating from CTA, PCL and polymer backbone). FT-IR (KBr): 3426, 2935, 2870, 1732, 1638, 1458, 1385, 1354, 1153, 1112, 1045, 957, 856, 688 $cm^{-1}$.

**Synthesis of poly(PEG-*co*-PCL)-*graft*-PNIPAM**

To a Schlenk tube were added G2 (0.69 g, 0.30 mmol of OH), PNIPAM (1.22 g, 0.18 mmol), pyridinium *p*-toluenesulfonate (PPTS, 0.015 g, 0.060 mmol), and dry DMF (9.5 mL) under nitrogen. The mixture was stirred at 40 °C for 36 h, and DMF was removed by distillation under reduced pressure. The crude product was partitioned between water and dichloromethane. After washing with $Na_2CO_3$ (5%) aqueous solution twice, the organic layer was collected and dried over $MgSO_4$ overnight. The polymer solution was concentrated and precipitated into diethyl ether thrice, and 1.28 g of graft copolymer (G3) was obtained after vacuum drying. $^1$H NMR analysis revealed that the number of grafted PNIPAM segments per copolymer ($m_{PNIPAM}$) was 5.7. Number-average molecular weight and polydispersity determined by GPC-MALLS were $M_{n,LS}$ = 78500, PDI = 1.18.

G3: $^1$H NMR ($CDCl_3$): $\delta$ 7.96, 7.56, 7.39 (m, Ph*H*), 5.7-7.2 (m, N*H* of PNIPAM), 4.5-4.9 (m, OC*H*($CH_3$)O and C*H*S), 4.2-4.4 (m, C*H*$_2$O), 4.06 (t, *J* 6.4, C*H*$_2$O of PCL), 4.00 (s, C*H*NH of PNIPAM), 3.82 (s, $COOCH_2CH_2$ connecting with PEG), 3.65 (s, $CH_2CH_2O$ of PEG and terminal C*H*$_2$OH of PCL), 3.47 (s, $CH_2OCHCH_3$), 3.38 (s, C*H*$_3$O), 0.5-3.0 (m, OCH(C*H*$_3$)O, and other C*H*, C*H*$_2$ and C*H*$_3$ resulting from CTA, PNIPAM and PCL). FT-IR (KBr): 3435, 3079, 2972, 2933, 2875, 1735, 1648, 1548, 1460, 1385, 1368, 1178, 1155, 1130, 1114, 1044, 841, 694 $cm^{-1}$.

**Formation of blank and DOX-loaded copolymer aggregates**

Under vigorous stirring, 1.0 mL of G3 solution ($c$ = 5.0 mg $mL^{-1}$, in DMSO) was added dropwise into 9.0 mL of phosphate buffered saline (PBS, pH 7.4, 50 mM) solution. Two hours later, the solution was transferred into dialysis membrane tubing (MWCO 3500) and dialyzed against PBS solution for 24 h to remove the organic solvent. The diameter and morphology of aggregates were determined by DLS and TEM.

To prepare DOX-loaded aggregates, G3 (10.0 mg) and DOX HCl (2.0 mg) were dissolved in 2.0 mL of DMSO, and followed by addition of about 0.6 mg of triethylamine and stirring for 2 h. The mixture was added dropwise to 18.0 mL of PBS solution (pH 7.4, 50 mM) and further stirred for 4 h. The resultant solution was dialyzed against PBS solution for 24 h (MWCO 3500), and the amount of DOX was determined using fluorescence (FLS920) measurement (excitation at 480 nm and emission at 560 nm). On the basis of fluorescence analysis, the drug loading capacity (DLC) of aggregates was calculated as the weight ratio of actual drug to drug-loaded aggregates, and the drug loading efficiency (DLE) of aggregates was calculated as the weight ratio of actual and added drug content.

Blank and DOX-loaded coaggregates formed from G3 and $\beta$-CD mixture in PBS solution at 25 or 37 °C were prepared according to similar methods via dialysis.

**Stimuli-triggered destabilization of copolymer aggregates and in vitro drug release from DOX-loaded aggregates**

The size change of G3 aggregates in response to 10 mM DTT in PBS solution (pH 5.3) was monitored by DLS measurement. DTT was directly added to 2.0 mL of G3 aggregates in PBS solution (50 mM) to achieve a final concentration at 10 mM. The solution was stirred at 37 °C, and the size at different time intervals was determined by DLS.

DOX-loaded G3 aggregates and G3/$\beta$-CD coaggregates were subjected to in vitro drug release. In a typical run, two portions of DOX-loaded G3 aggregates in PBS solution (4.0 mL, pH 7.4) were put into a dialysis bag (MWCO 5000), which were then immersed into 20 mL of (a) PBS solution (50 mM, pH 7.4) with 10 mM DTT or (b) normal PBS solution (50 mM, pH 7.4) at 37 °C. At predetermined time intervals, the drug-release solution was changed, and the amount of DOX released from aggregates was measured by fluorescence measurement (excitation at 480 nm) at room temperature. All release experiments were performed in triplicate.

**In vitro cytotoxicity assay**

Free G3 aggregates, DOX-loaded G3 aggregates, and DOX-loaded G3/$\beta$-CD coaggregates were seeded in 96-well plates at the density of $3 \times 10^4$ cells/wells and incubated in 100 μL of medium at 37 °C in 5% $CO_2$ for 24 h. DOX was dissolved in DMSO and diluted into DOX aqueous solution with specific concentration. On this basis, the cells were separately incubated in culture media containing DOX,

 

G3, DOX-loaded G3 and G3/*β*-CD micelles with different concentrations (each one with 3 plates). After 4-h incubation, medium was removed and then replaced with fresh one. The medium was replaced by 20 μL of MTT solution (2.5 mg $mL^{-1}$) and then incubated at 37 °C in dark. Four hour later, MTT medium was removed from each well and 100 μL of DMSO was added, and then the mixture was stirred at room temperature. The optical density (OD) at 490 nm was measured on a Victor3 1420 multilabel counter (Perkin-Elmer, USA).

**Intracellular distribution using confocal laser scanning microscopy (CLSM)**

4T1 cells ($1\times10^5$ cells) were cultured in 35 mm culture dishes containing 4 mM DOX-loaded G3 micelles for different times. After washing with PBS (pH 7.4) for three times, cells were labeled with 4',6-diamidino-2-phenylindole (DAPI) and then imaged by a laser scanning confocal fluorescencemicroscope (Leica SP5), to determine the cellular uptake of DOX-loaded S2 micelles.

**Characterization**

The apparent number-average molecular weight ($M_{n,GPC}$) and polydispersity (PDI) of PNIPAM and G1 were measured on a Waters 150-C gel permeation chromatography (GPC) using three Ultrastyragel columns with 10 μm bead size at 35 °C. THF was used as an eluent at a flow rate of 1.0 mL $min^{-1}$, and the samples were calibrated with PMMA standard samples. Gel permeation chromatography with multiple angle laser scattering detection (GPC-MALLS) system was used to determine the absolute number-average molecular weight ($M_{n,LS}$) and polydispersity of G2 and G3. GPC was conducted in THF at 35 °C with a flow rate of 1.0 mL $min^{-1}$, and three TSK-GEL H-type columns with 5 μm bead size were used. Data were collected and processed by use of ASTRA software from Wyatt Technology, and molecular weights were determined by the triple detection method. $^1H$ (400 MHz) and $^{13}C$ (100 MHz) NMR spectra were recorded on a Varian spectrometer at 25 °C using $CDCl_3$ or DMSO-$d_6$ as a solvent. Fourier Transform Infrared (FT-IR) spectra were recorded on a Perkin-Elmer 2000 spectrometer using KBr discs. Differential scanning calorimetry (DSC) analysis was performed under a nitrogen atmosphere on Q200 DSC (TA Instruments - Waters LLC) with a heating rate of 10 °C $min^{-1}$. Dynamic light scattering (DLS) measurements were conducted at 25 °C using Zetasizer Nano-ZS from Malvern Instruments equipped with a 633 nm He–Ne laser using back-scattering detection. Transmission electron microscopy (TEM) images were obtained through a Hitachi H-600 electron microscope.

## Results and discussion

**Synthesis and characterization of graft copolymer**

First, vinyloxy-terminated PNIPAM was synthesized by RAFT polymerization mediated by 4-(vinyloxy)butyl 4-cyano-4-(phenylcarbonothioylthio)pentanoate (VCP, Fig. S1 and Fig. S2). RAFT polymerization ($[NIPAM]_0:[VCP]_0:[AIBN]_0$ = 70:1:0.2) performed in dioxane at 70 °C for 18 h gave PNIPAM in 81.0% conversion. In $^1H$ NMR spectrum of PNIPAM (Fig. S3), characteristic signals of NIPAM unit were noted at 4.00 (NHC*H*), 2.14 (COC*H*) and 1.13 ppm ($CH_3$), and signals of terminal Ph*H* and $CH_2OCH{=}CH_2$ were observed at 7.96, 7.56, and 7.39 (Ph*H*), 3.9-4.2 (OCH=C$H_2$) and 3.66 ppm (C$H_2$O) although the signal of CH at around 6.5 ppm was overlapped with that of NH in PNIPAM. By comparing the integral areas at 7.96 and 4.00 ppm, the degree of polymerization ($DP_{PNIPAM}$ = $2I_{3.8\text{-}4.3}/I_{7.96} - 4$) was determined to be 56.4. The molecular weight given by $^1H$ NMR analysis ($M_{n,NMR}$ = 6750) was close to the expected value ($M_{n,th}$ = 6780), and no significant shoulder and tailing was noted in GPC trace (Fig. 1). Characteristic absorption bands appeared at 3072 ($\nu_{NH}$), 1650 ($\nu_{C=O}$), and 1544 ($\delta_{NH}$) $cm^{-1}$ in IR spectrum of PNIPAM (Fig. S4).

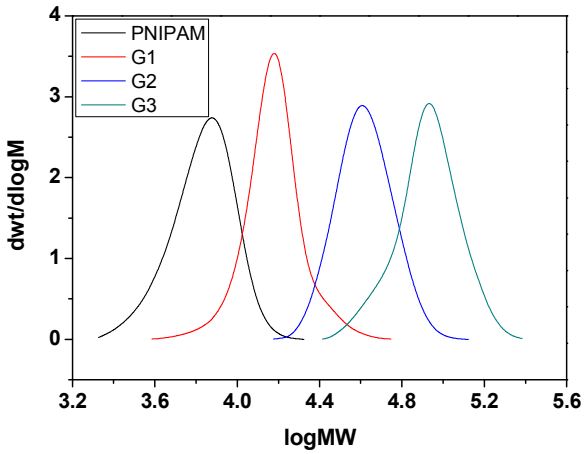


**Fig. 1** GPC traces of PNIPAM, poly(HEMA-*co*-PEGMEMA) (G1), poly(PEG-*co*-PCL) (G2), and poly(PEG-*co*-PCL)-*graft*-PNIPAM (G3).

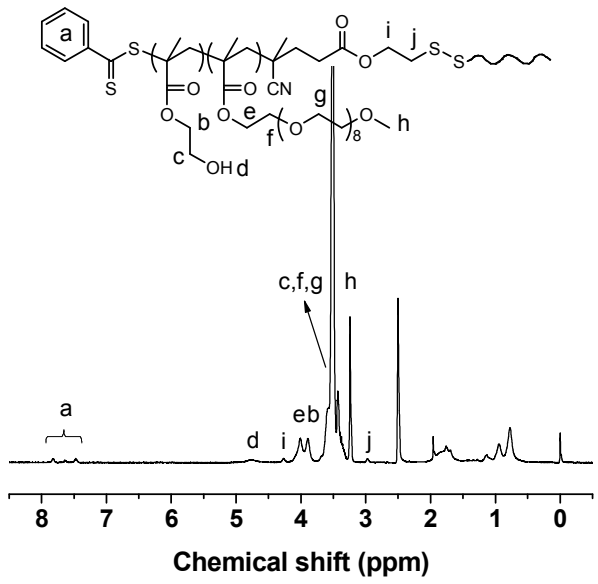


**Fig. 2** $^1H$ NMR spectrum of disulfide-linked poly(HEMA-*co*-PEGMEMA) (the wavy line denotes the another half of the random copolymer except the disulfide linkage).

Second, disulfide-linked copolymer poly(HEMA-*co*-PEGMEMA) (G1) was synthesized by S-CPDB mediated RAFT copolymerization.

RAFT process ([HEMA]$_0$:[PEGMEMA]$_0$:[S-CPDB]$_0$:[AIBN]$_0$ = 20:20:1:0.4) performed in DMF at 60 °C for 8 h gave G1 in 90.3% conversion. The isolated copolymer exhibited monomodal distribution in GPC trace, and the polydispersity index was 1.11 (Fig. 1). In $^1$H NMR spectrum of G1 (Fig. 2), signals of HEMA unit appeared at 4.77 ($CH_2OH$), 3.89 ($COOCH_2$), and 3.58 ppm ($CH_2OH$), signals of PEGMEMA unit were noted at 4.01 ($COOCH_2$), 3.51 ($CH_2CH_2O$), 3.43 ($COOCH_2CH_2O$), and 3.24 ppm ($CH_3O$), and signals originating from dithiobenzoate and disulfide linkage appeared at 7.82, 7.64, 7.47 (Ph$H$), 4.26 ($SCH_2CH_2OCO$), and 2.97 ppm ($SCH_2CH_2OCO$). Based on the equations $DP_2 = 2I_{3.24}/(3I_{7.82})$ and $DP_1 = I_{3.75\text{-}4.2}/I_{7.82} - DP_2$, polymerization degree of HEMA ($DP_1$) and PEGMEMA ($DP_2$) were calculated to be 18.0 and 18.2, respectively.

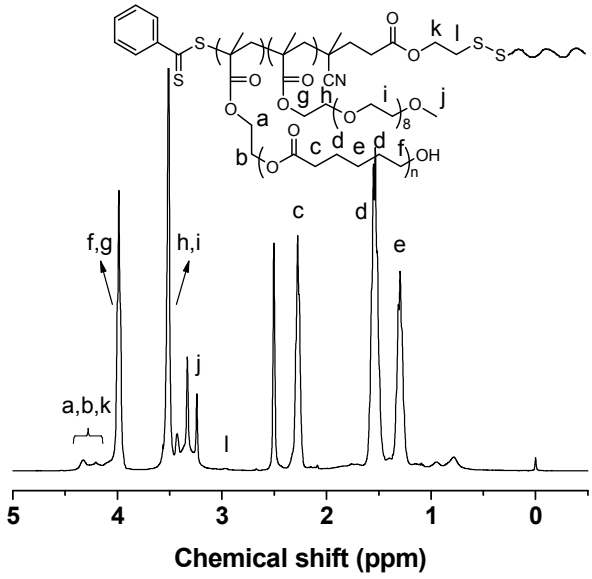


**Fig. 3** $^1$H NMR spectrum of disulfide-linked comblike poly(PEG-*co*-PCL) with polymethacrylate backbone (the wavy line denotes the another half of the graft copolymer except the disulfide linkage).

Third, G1 was used as a macroinitiator for CL polymerization to generate disulfide-linked comblike copolymer poly(PEG-*co*-PCL) (G2). When ROP ([CL]$_0$:[OH]$_0$:[Sn(Oct)$_2$]$_0$ = 15:1:0.1) was conducted in toluene at 90 °C for 24 h, G2 was isolated in 94.2% conversion after precipitating into methanol. In $^1$H NMR spectrum of G2 (Fig. 3), signals of PEG segments were noted at 3.51 ($CH_2CH_2O$) and 3.24 ppm ($CH_3O$), and signals of PCL segments appeared at 3.99 ($CH_2O$), 2.28 ($CH_2COO$), 1.55 and 1.30 ppm (other $CH_2$). The signals of HEMA units at 4.77 ($CH_2OH$), 3.89 ($COOCH_2$), and 3.58 ppm ($CH_2OH$) were absent, and a new signal was almost quantitatively noted at 4.33 ppm ($COOCH_2CH_2O$ connecting with PCL chains), which indicated the ring-opening polymerization was highly efficient performed. Based on polymerization degree of PCL segments calculated by comparing the integral areas at 4.33 and 2.28 ppm ($DP_{PCL} = 2I_{2.28}/I_{4.33}$), the number-average molecular weight ($M_{n,NMR}$ = 41300) and PCL content ($f_{w,PCL}$ = 0.717) were obtained. Number-average molecular weights of G2 determined by GPC-MALLS ($M_{n,LS}$ = 39200) and NMR ($M_{n,NMR}$) were comparable, and both were close to theoretical molecular weights ($M_{n,th}$ = 40700). The GPC trace of G2 as listed in Fig. 1 was of symmetric distribution, with relatively low polydispersity (PDI = 1.13).

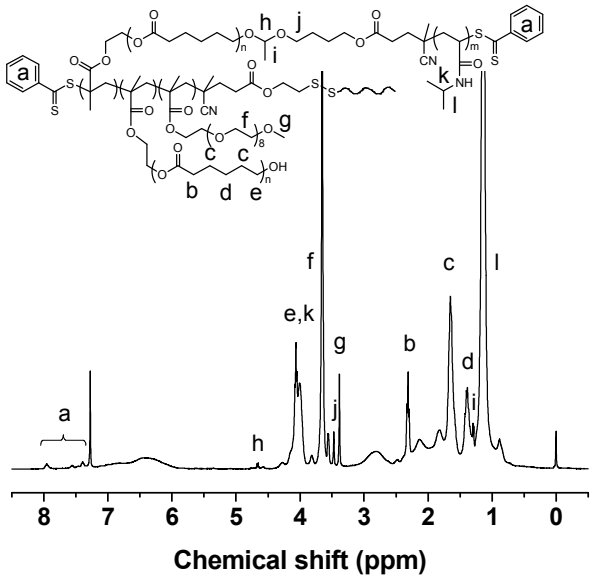


**Fig. 4** $^1$H NMR spectrum of acetal and disulfide functionalized comblike poly(PEG-*co*-PCL)-*graft*-PNIPAM copolymer (the wavy line denotes the another half of the graft copolymer except the disulfide linkage).

Last, comblike copolymer poly(PEG-*co*-PCL)-*graft*-PNIPAM (G3, $M_{n,LS}$ = 78500, PDI = 1.18) was generated by hydroxyl-vinyloxy adductive reaction. Vinyloxy-functionalized PNIPAM and hydroxyl-functionalized G2 ([OH]$_0$:[PNIPAM]$_0$:[PPTS]$_0$ = 5:3:1) were subjected to reaction in DMF at 40 °C for 36 h, and ungrafted PNIPAM was efficiently removed by extraction. In $^1$H NMR spectrum of isolated G3 (Fig. 4), characteristic signals originating from graft reaction appeared at about 4.67 ($OCH(CH_3)O$) and 1.30 ppm ($OCH(CH_3)O$), and signals of various segments were noted at 4.06, 2.31, 1.65, 1.38 ($CH_2$ of PCL), 4.00, 2.13, 1.14 (C$H$ and $CH_2$ of PNIPAM), 3.65, and 3.38 ppm ($CH_2$ and $CH_3$ of PEG). By comparing the integrated areas at 1.14 ($CH_3$ of PNIPAM) and 3.65 ($CH_2O$ of PEG), the numbers of grafted PNIPAM segments ($m_{PNIPAM}$) were determined to be 5.7, revealing about 32% of PCL segments were converted into acetal-bridged PEG-*b*-PNIPAM grafts. Careful inspection of Fig. 4 also revealed that the signals of protons in PCL segments were partly weakened, possibly originating from the shielding effect. On the basis of $^1$H NMR analysis, the $M_{n,NMR}$ value of G3 was calculated as 77600, and PCL content was deduced to be 0.381. The $M_n$ values given by $^1$H NMR and GPC-MALLS were similar, and the GPC trace of G3 completely shifted to higher molecular weight side than its precursors (Fig. 1). In IR spectrum (Fig. S4), characteristic absorption bands of various segments were observed at 1735 ($\nu_{C=O}$ of PCL), 1648 ($\nu_{C=O}$ of PNIPAM), 1548 ($\delta_{NH}$ of PNIPAM), and 1114 ($\nu_{C\text{-}O}$ of PEG) cm$^{-1}$. These results confirmed the target graft copolymer was successfully obtained via adductive

**Table 2** Properties of copolymer aggregates formed by G3 and G3/*β*-CD mixture ($c_{polymer}$ = 0.50 mg mL$^{-1}$, $c_{\beta\text{-CD}}$ = 1.0 mM) in PBS solution (pH 7.4, 50 mM) at 37 °C

| sample | $D_h$ (nm)[a] | PD[a] | $D_{peak}$ (nm)[a] | $D_h$ (nm)[b] | PD[b] | $D_{peak}$ (nm)[b] | DLC (%) | DLE (%) |
|---|---|---|---|---|---|---|---|---|
| G3 | 306 | 0.060 | 330 | 183 | 0.095 | 199 | 4.72 | 23.6 |
| G3 + *β*-CD | 136 | 0.130 | 152 | 158 | 0.095 | 175 | 6.23 | 31.2 |

[a] Hydrodynamic diameter ($D_h$), particle size distribution (PD), and peak size ($D_{peak}$) of blank copolymer aggregates obtained by DLS analyses. [b] $D_h$, PD and $D_{peak}$ values of DOX-loaded aggregates given by DLS analyses.

reaction. Owing to its relatively high efficiency,[24,25] this method has a great potential to synthesize graft copolymers with tunable number of acetal-linked block-type pendent chains and hydrophilic / hydrophobic ratios.

The glass transition, melting and crystallization behaviors of G3 and its precursors were investigated by differential scanning calorimetry (DSC, Table 1). PNIPAM exhibited a glass transition temperature ($T_g$) at 116.0 °C, and G1 had two $T_g$s at -46.3 and -12.2 °C corresponding to chain relaxation of oligomeric PEG and polymethacrylates backbone (Fig. S5). G2 possessed two glass transitions at -71.6 ($T_{g,PCL}$) and -51.7 °C ($T_{g,PEG}$) and two melting peaks of PCL grafts at 21.4 and 29.0 °C, in which the reduced $T_g$ of PEG segments could be partly ascribed to the enhanced branching effect. Careful inspection of DSC trace of G3 revealed three weak glass transitions at around -63.7 ($T_{g,PEG/PCL}$), -15.1 ($T_{g,backbone}$), and 112.5 °C ($T_{g,PNIPAM}$), suggesting the partial compatibility among PEG, PCL and PNIPAM segments. The degree of crystallinity ($X_c$) of PCL segment was only about 6.4% although the weight percent of PCL reached up to 71.7% in G2, while no notable melting peak was noted in DSC trace of G3. These results indicated that the presence of PEG and PNIPAM segments could significantly prevent PCL chains from folding and rearrangement, and thus it was difficult to form crystallization regions.

**Formation of G3 and G3/*β*-CD (co)aggregates and stimuli-triggered morphological transition of G3 aggregates**

Dual-cleavable graft copolymer G3 was chosen as a typical sample to reveal the influence of various factors on aggregation behaviors and drug release properties (Table 2). Meanwhile, coassembly of G3 (0.50 mg mL$^{-1}$) and *β*-CD (1.0 mM) mixture was also performed to investigate the potential of coaggregates in smart drug delivery systems. After self-assembly in aqueous solution to form copolymer aggregates, DLS was used to determine their average hydrodynamic diameter ($D_h$), peak size with the highest intensity ($D_{peak}$) and particle size distribution (PD). The aggregates only exhibited monomodal distribution in DLS plots (Fig. 5 and Fig. 6), and their apparent particle parameters ($D_h$, $D_{peak}$, and PD) were obtained as 179 nm, 198 nm, 0.090 (for G3 aggregates at 25 °C), 306 nm, 330 nm, 0.060 (for G3 aggregates at 37 °C) and 136 nm, 152 nm, 0.130 (for G3/*β*-CD coaggregates at 37 °C). TEM images revealed that G3 aggregates (T = 25 °C, Fig. 7a) and G3/*β*-CD coaggregates (T = 37 °C, Fig. S6) were spherical micelles, and G3 aggregates at 37 °C were similar to the toroidal micelles originating from thermo-induced morphological change (b and c of Fig. 7). Although the sizes of G3 aggregates given by DLS and TEM were roughly comparable, the hydrodynamic diameters of G3/*β*-CD coaggregates estimated by two methods were quite different ($D_{h,TEM}$ ≈ 100 nm, and $D_{h,DLS}$ = 136 nm, Fig. S6). This

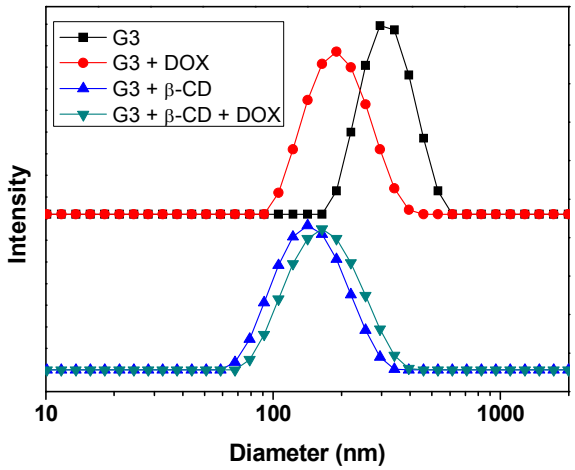


**Fig. 5** DLS plots of blank and DOX-loaded aggregates ($c_{polymer}$ = 0.50 mg mL$^{-1}$, $c_{\beta\text{-CD}}$ = 1.0 mM) formed from G3 and G3/*β*-CD mixture in PBS solution (pH 7.4, 50 mM) at 37 °C.

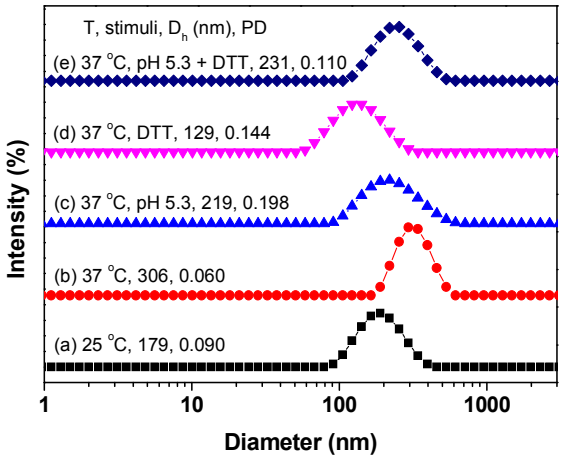


**Fig. 6** Influence of temperature and other stimuli (pH 5.3, 10 mM DTT) on DLS plots of G3 aggregates ($c$ = 0.50 mg mL$^{-1}$) formed in PBS solution (pH 7.4 or 5.3, 50 mM), in which the aggregates in runs c-e were treated with external stimuli for 24 h.

phenomenon was possibly originated from the significant shrinkage of nanostructures at the dry state, in which the presence of $\beta$-CD potentially allowed for increased hydrogen-bonding and host-guest interactions among $\beta$-CD, PEG and PCL, and the supramolecular self-assembly using bulky building blocks was liable to form coaggregates with looser packing of polymer segments.

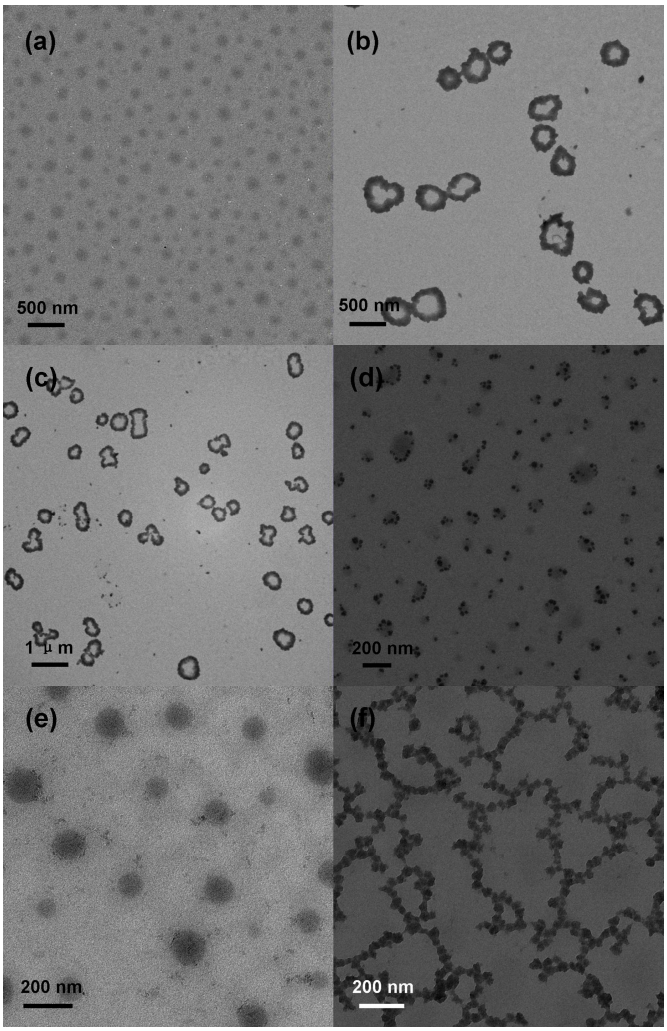


**Fig. 7** TEM images of G3 aggregates ($c$ = 0.50 mg mL$^{-1}$) formed at different conditions: (a) 25 $^{o}$C; (b, c) 37 $^{o}$C; (d) 37 $^{o}$C + pH 5.3 for 24 h; (e) 37 $^{o}$C + 10 mM DTT for 24 h; (f) 37 $^{o}$C + pH 5.3 + 10 mM DTT for 24 h.

On this basis, stimuli-triggered morphological transition of G3 aggregates at 37 $^{o}$C was preliminarily investigated. As temperature increased from 25 to 37 $^{o}$C, the morphology of G3 aggregates changed from spherical micelles (Fig. 7a) to toroidal micelles (b and c of Fig. 7), and the morphology transition was possibly ascribed to the synergistic effect of increasing hydrophobicity of PNIPAM segments at a temperature beyond LCST and varied intensity and ratio of inter- and intramolecular interactions such as hydrophobic and hydrogen-bonding interactions. At 37 $^{o}$C, the spherical micelles were necessary to bear large chain packing frustration since PNIPAM segments became hydrophobic, and thus intermicellar interaction took place to allow the formation of more stable toroids with less interfacial curvature.[75–81] TEM images showed predominantly toroidal micelles besides spherical and cylindrical micelles (b and c of Fig. 7). Taking into account that the apparent $D_h$ values given by DLS were in the range 90-600 nm, the residual spherical and curved cylindrical micelles may be formed during sample drying due to disassembly and fusion of toroidal micelles, leading to the differences in sizes of aggregates given by DLS and TEM analyses. The cross-sectional diameter of the rings was around 110 nm, and the ring size diameter ranging from 280 to 900 nm had an average value of about 450 nm. The ring sizes of G3 toroids were larger than those based on block copolymers[75–80] and close to those formed by Rhodamine B end-capped PNIPAM in chloroform at 40 $^{o}$C.[81] The large ring sizes were possibly ascribed to the relatively weak interactions among PNIPAM and other segments at 37 $^{o}$C, which were difficult to sustain the high bending strains of small rings.[81] Careful inspection of the toroids revealed that the rings comprised undulations in the cross-section, indicating that the rings were possibly formed through coalescence of spherical micelles and/or cylindrical micelle endcaps.[75–77] These results supported the results that spherical micelles could be transformed into a toroidal structure by increasing the volume fraction of hydrophobic segments reported by Lee and coworkers.[79,80]

As G3 aggregates formed at 37 $^{o}$C were treated with acid stimulus (pH 5.3) for 24 h, aggregates similar to multicompartment micelles (Fig. 7d) were obtained. Compared with original toroidal micelles, aggregates formed in the presence of acid had decreased size ($D_h$ = 219 nm) and broadened particle size distribution (PD = 0.198, Fig. 6c). The morphological transition could be attributed to acid-induced degradation and reassembly of cleaved copolymers, in which the black dots on the edge of aggregates revealed the presence of microphase separation (Fig. 7d). Under acidic conditions, the detachment of PNIAM segments from PCL chains resulting from cleavage of acetal linkages led to the formation of mixtures containing PNIPAM and graft copolymer with PEG and PCL grafts, and the coaggregation was performed until stable coaggregates were formed. The aggregates obtained were very stable, and no PNIPAM was precipitated during reassembly at 37 $^{o}$C, revealing the cleaved PNIPAM segments and graft copolymers could efficiently interact with each other via hydrophobic interactions in acidic solution. The size given by DLS was larger than that determined by TEM, and the size distribution seemed wide in TEM image. One possible reason lay in much stronger interactions among coaggregates in acidic solution than that in dry state, in which part of aggregates may disassemble to form smaller nanoobjects during sample preparation.

Upon reduction stimulus (10 mM DTT) for 24 h, the disulfide linkage in polymer backbone was completely cleaved, and spherical micelles (Fig. 7e) with reduced size ($D_h$ = 129 nm, Fig. 6d) were formed. Reduction-triggered formation of spherical micelles was originated from the reaggregation of cleaved thiol-bearing graft copolymers,[24,25,70,71] which had end group and molecular weight different from their precursors. As G3 micelles were treated with dual stimuli (pH 5.3 and 10 mM DTT) at 37 $^{o}$C for 24 h, the aggregates formed from cleaved copolymers were similar to "hyperbranched" or "necklace"-like cylinders[82] (Fig. 7f) with apparent size of 231 nm (Fig. 6e). The morphological transition upon dual stimuli was more complex due to the remarkable changes in microenvironment including molecular weight, chemical composition, polymeric topology and end group. These factors were

liable to form distinct inter- and intramolecular interactions, which further induced the destabilization and reaggregation of polymeric coaggregates comprising PNIPAM and thiol-terminated graft copolymer until a thermodynamic equilibrium was reached.[11–25] The drastic changes in morphologies and sizes of copolymer aggregates upon external stimuli are liable to result in tunable solution and interface properties, and these multi-sensitive aggregates may have potential applications in SDRS and functional surface and interface materials.

**Stimuli-triggered in vitro drug release from DOX-loaded copolymer aggregates**

To reveal the potential of multi-sensitive graft copolymer in bioscience, loading and release of DOX from G3 and G3/*β*-CD aggregates were investigated. A model anticancer drug DOX was chosen and encapsulated into copolymer aggregates by dialysis method. After loading the drug at 37 °C, the hydrodynamic sizes of DOX-loaded aggregates were about 183 (for G3) and 158 nm (for G3/*β*-CD), and unimodal distribution with low PD value (PD = 0.095) was noted in DLS plots (Table 2 and Fig. 5). As determined by fluorescence analysis, the drug loading capacity (DLC) and drug loading efficiency (DLE) of DOX-loaded G3 aggregates were 4.72% (for DLC) and 23.6% (for DLE), which were lower than those of G3/*β*-CD coaggregates (DLE = 31.2%). On this basis, stimuli-triggered drug release properties of DOX-loaded aggregates were investigated, and acid, reduction and thermo stimuli were applied to reveal the effects of external stimuli on drug release properties (Table S1).

The in vitro drug releases from G3 aggregates were performed in PBS solution (50 mM, pH 7.4 or 5.3) with or without 10 mM DTT at 25 or 37 °C for 48 h. The maximum release rate at a fixed temperature was liable to decrease in the order pH 5.3 + DTT > pH 5.3 > DTT > lack of stimulus, and the apparent release rate (*K*) derived from the release profiles was in the range of 0.072-0.186 $h^{-1}$ at 25 °C and 0.163-0.403 $h^{-1}$ at 37 °C (a and b of Fig. 8). The cumulative release amount (CR) at 48 h was 36.1% (25 °C + pH 7.4), 59.9% (25 °C + pH 5.3 + DTT), 48.3% (37 °C + pH 7.4), 67.4% (37 °C + pH 7.4 + DTT), 63.0% (37 °C + pH 5.3), and 77.1% (37 °C + pH 5.3 + DTT), and the increment of cumulative release (ICR, defined as the enhanced percent as compared with the lowest cumulative release amount at a fixed time) was in the range of 33.8-114% under different conditions. The release rate of DOX from G3 aggregates at 37 °C was much faster than that at 25 °C, which could be partly ascribed to the improved solubility of DOX in water at higher temperature. Moreover, the release kinetics could be further accelerated as acid and reduction stimuli were applied, revealing the critical roles of external stimuli during release process. As well documented, acid condition favored the cleavage of acetal linkages, and reduction environment was liable to cleave the disulfide linkage, resulting in the gradual production of lower-molecular-weight PNIPAM and graft polymers.[11–25] The change in microenvironment such as molecular weight, end group, and hydrophobic/hydrophilic ratio could further induce the copolymer aggregates to perform destabilization and reaggregation, evident from the results of DLS plots monitored at 37 °C. In the absence of external stimuli, G3 aggregates could be stably stood for a long period of time, and no remarkable change in D and PD was noted in 48 h. Upon dual stimuli (pH 5.3 + 10 mM DTT), the average hydrodynamic diameter of G3 aggregates gradually increased from 187 (t = 1 h) to 239 nm (t = 48 h), and the particle size distribution was fluctuated between

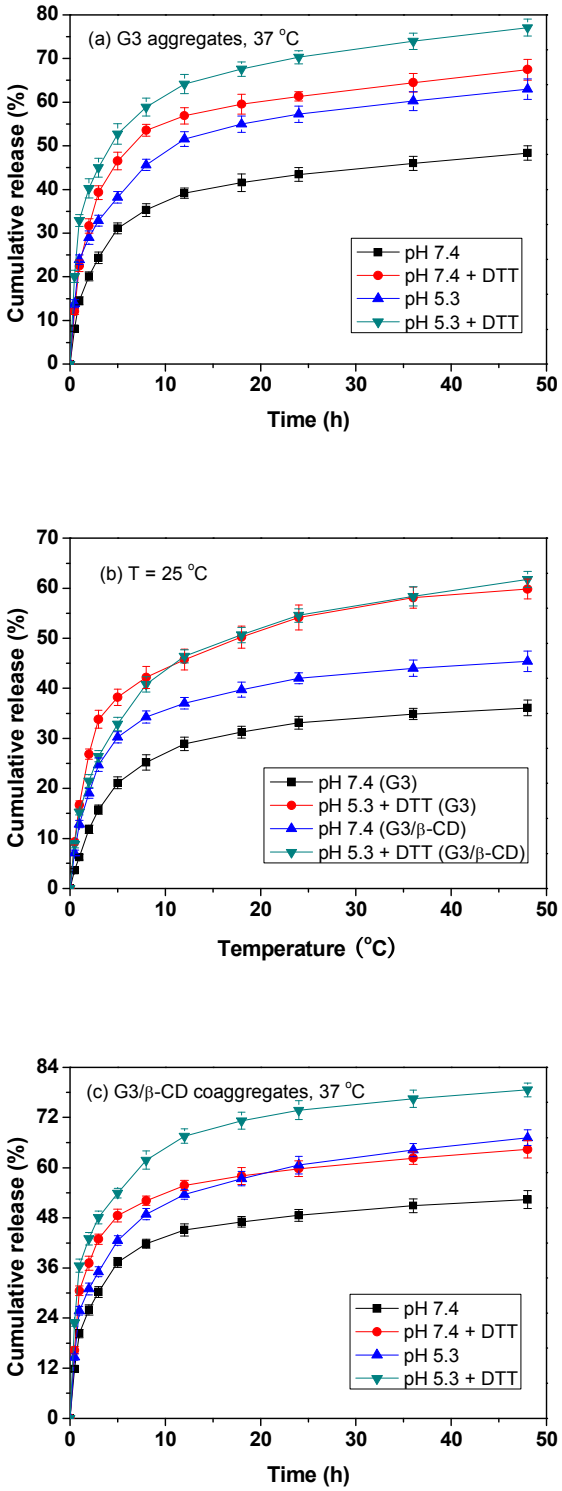


**Fig. 8** In vitro drug release profiles of DOX-loaded G3 and G3/*β*-CD aggregates ($c_{polymer}$ = 0.50 mg $mL^{-1}$, $c_{\beta\text{-CD}}$ = 1.0 mM) in PBS solution (50 mM, pH 7.4 or 5.3) with or without addition of 10 mM DTT at 25 or 37 °C.

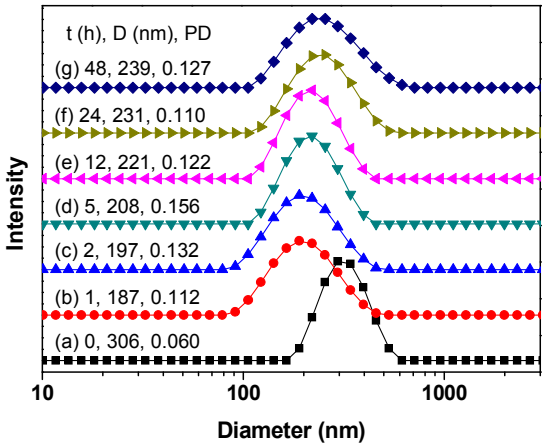


**Fig. 9** DLS plots of G3 aggregates ($c$ = 0.50 mg mL$^{-1}$) with (b-g, pH 5.3 + 10 mM DTT) or without (a, pH 7.4) external stimuli in PBS solution (50 mM) at 37 °C for different time periods.

0.110 and 0.156 (b-g of Fig. 9). Although monomodal distribution was observed in each case, the continually increased sizes and slightly broadened distribution in DLS plots revealed the destabilization of copolymer aggregates was dynamically performed due to the change in microenvironment. Therefore, the encapsulated drug could be faster released from the aggregates during reaggregation among various polymer segments. These results indicated that the release kinetics of DOX-loaded G3 aggregates could be efficiently adjusted in a wide range by choosing different stimuli.

Meanwhile, the in vitro drug releases from G3/*β*-CD coaggregates were investigated to reveal the potential of aggregates bearing host-guest interaction in drug delivery systems. As well known, the coassembly of graft copolymer and *β*-CD allowed for alteration of the strength of hydrogen-bonding interactions and van der Waals forces and formation of host-guest interactions among *β*-CD, PEG and PCL segments.[41–60] At 25 °C, G3/*β*-CD coaggregates ($K$ = 0.142 h$^{-1}$) exhibited faster release kinetics than G3 aggregates ($K$ = 0.072 h$^{-1}$) at pH 7.4, which could be attributed to the differences in mutual interactions and packing density of copolymer aggregates. With the introduction of *β*-CD, the host-guest interactions among *β*-CD and pendent grafts could dynamically perform, and the hydrophobic interactions between PCL segments and hydrophobic drug were weakened. Meanwhile, *β*-CD-bearing coaggregates were liable to be loosely packed due to the bulky side chains. Both factors could result in accelerated release of encapsulated DOX. With addition of dual stimuli, the $K$ and CR values of G3/*β*-CD coaggregates at 25 °C were roughly comparable to those of G3 aggregates although the cumulative release of G3 aggregates was higher than coaggregates within the initial 8 h. By comparing the release plots of aggregates with or without external stimuli (pH 5.3 + 10 mM DTT), it can be seen that the addition of dual stimuli normally afforded significantly accumulated release kinetics, but the $K$ and CR values for G3/*β*-CD coaggregates were only slightly increased within the initial 5 h at 25 °C (Fig. 8b). This phenomenon was potentially ascribed to the critical role of *β*-CD, which could not only interact with DTT via supramolecular interactions but hinder DTT from approaching disulfide linkage to perform the cleavage reaction. Therefore, the accumulated release process in coaggregates at 25 °C was lagged behind than the release system based on G3 aggregates. As the releases from coaggregates were performed at 37 °C, the $K$ (h$^{-1}$) values were liable to decrease in the order pH 5.3 + DTT (0.458) > pH 7.4 + DTT (0.325) > pH 5.3 (0.293) > pH 7.4 (0.236), and the cumulative releases at 48 h were in the range of 52.4-78.6%. Careful inspection of Fig. 8c revealed that the CR value with DTT at pH 7.4 was more or less larger than that at pH 5.3 within the initial 18 h, and then the latter went beyond the former in 24 h. These results confirmed that the drug releases from G3/*β*-CD coaggregates were strongly dependent on the external stimuli.

The above-mentioned results revealed that the $K$ and CR values of various aggregates could be adjusted in a wide range by choosing different types of external stimuli. Owing to the presence of thermo-responsive PNIPAM segments and dually cleavable linkages, both G3 aggregates and G3/*β*-CD coaggregates could efficiently exhibit triply sensitive drug release properties. The blank and DOX-loaded aggregates could be stably stood for at least one week, and no notable precipitation appeared during the release process. Consequently, these multi-responsive copolymer aggregates had a great potential in versatile nanocarriers for SDRS.

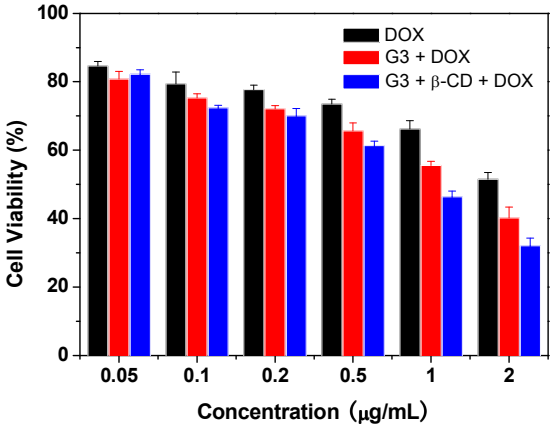


**Fig. 10** Cell viability of 4T1 cells incubated with free DOX or DOX-loaded aggregates at various concentrations at 37 °C for 24 h. Error bars denote standard deviations from three parallel trials.

### Cytotoxicity of DOX-loaded aggregates and CLSM images of 4T1 cells

The cytotoxicity and anticancer efficiency of *β*-CD solution, blank and DOX-loaded G3 micelles and DOX-loaded G3/*β*-CD coaggregates were investigated in 4T1 cells using MTT assay. No obvious cytotoxicity was observed for G3 micelles at a concentration up to 0.2 mg mL$^{-1}$ (Fig. S7) and *β*-CD solution at a concentration up to 0.5 mg mL$^{-1}$ (Fig. S8). In contrast, both DOX-loaded G3 micelles and G3/*β*-CD coaggregates showed enhanced cytotoxicity with increasing concentration, and the viability of 4T1 cells decreased in the order G3/*β*-CD/DOX > G3/DOX > free DOX as the concentration of DOX was beyond 0.1 μg mL$^{-1}$ (Fig. 10), revealing DOX-loaded aggregates were liable to exhibit higher efficiency in

killing cancer cells than free DOX. One possible reason laid in relatively strong interactions between G3 and *β*-CD, which could more tightly encapsulate DOX during aggregation and result in enhanced endocytosis. Meanwhile, obvious co-localization of DOX-loaded aggregates' fluorescence with lysotracker signals was observed (Fig. 11), indicating that DOX-loaded G3 micelles were primarily located in lysosomes and cell nuclei after cell uptake. Therefore, it is likely that DOX-loaded copolymer aggregates may enter cells by endocytosis according to a nanocomplex manner.

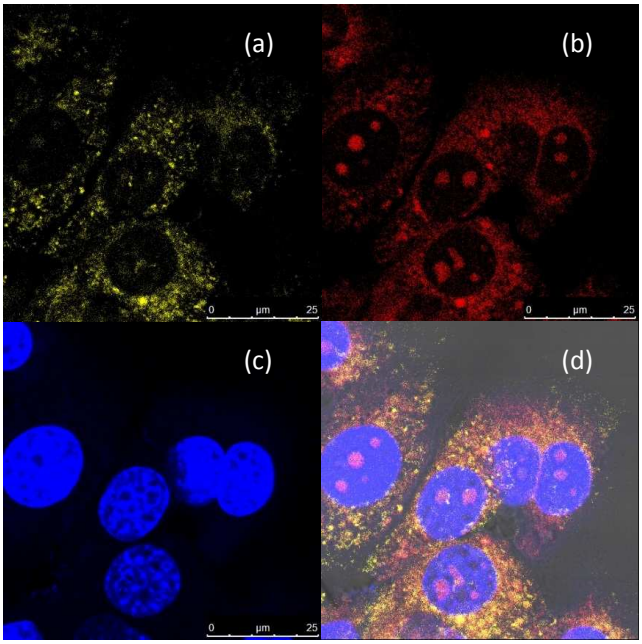


**Fig. 11** Confocal fluorescence images of 4T1 cells incubated with 4 mM DOX-loaded G3 micelles for 2 h: (a) lysosomes stained by Lysotracker Red DND-99, (b) G3 micelles with red fluorescence from DOX, (c) cell nuclei stained by 4',6-diamidino-2-phenylindole, and (d) co-localization of micelles within the lysosomes.

## Conclusions

A poly(PEG-*co*-PCL)-*graft*-PNIPAM copolymer with one disulfide linkage and multiple acetal moieties was synthesized by combination of RAFT process, ROP and hydroxyl-vinyloxy adductive reaction. The versatile method allowed for controlled synthesis of the target graft copolymer with low polydispersity and tunable number of stimuli-responsive polymer segments. DSC analysis revealed PEG, PCL and PNIPAM grafts were partly compatible, while no melting peak of PCL segments was noted due to remarkably restricted chain folding and rearrangement. Both G3 and G3/*β*-CD mixture could self-assemble into stable aggregates in aqueous solution at 25 and 37 $^{o}$C. Owing to the gradual change in microenvironment involving molecular weight, end group, and hydrophobic/ hydrophilic ratio, the in vitro release kinetics from DOX-loaded aggregates could be efficiently adjusted in a wide range by applying acid, reduction and thermo stimuli, in which the apparent release rate under different conditions was within the range of 0.072-0.403 $h^{-1}$ for G3 aggregates and 0.142-0.458 $h^{-1}$ for G3/*β*-CD coaggregates. These stimuli-sensitive copolymer aggregates had a great potential in smart drug delivery systems due to their reasonable drug loading efficiency and multi-triggered release properties. The results demonstrated that the introduction of acid and reduction cleavable linkages and stimuli-responsive segments could efficiently construct multi-sensitive drug release systems, and the application of host-guest interactions bearing *β*-CD could further adjust the release kinetics. Although *β*-CD and G3 micelles did not exhibit significant cytotoxicity, DOX-loaded copolymer aggregates had higher cytotoxicity to 4T1 cells as compared with free DOX. CLSM images revealed that DOX-loaded copolymer aggregates may act as nanocomplex to enter cells via endocytosis. Our preliminary results revealed that both G3 aggregates and G3/*β*-CD coaggregates had a great potential as promising vehicles for multi-responsive drug delivery.

## Acknowledgements

This work was financially supported by the National Natural Science Foundation of China (Grants 21074081, 21274096 and 21474070), and the Project Funded by the Priority Academic Program Development of Jiangsu Higher Education Institutions. The authors are grateful to Professors Huabing Chen and Zhuang Liu at Soochow University for valuable discussion and kind help during cytotoxicity and CLSM measurements.

## Notes and references

*Suzhou Key Laboratory of Macromolecular Design and Precision Synthesis, Jiangsu Key Laboratory of Advanced Functional Polymer Design and Application, College of Chemistry, Chemical Engineering and Materials Science, Soochow University, Suzhou 215123, China. Tel: +86-512-65882045; Fax: +86-512-65882045; E-mail: ylzhao@suda.edu.cn*

† Electronic Supplementary Information (ESI) available: [NMR and IR spectra, DSC traces, and cell viability of 4T1 cells]. See DOI: 10.1039/b000000x/

1 C. D. H. Alarcón, S. Pennadam and C. Alexander, *Chem. Soc. Rev.*, 2005, **34**, 276–285.
2 R. K. O'Reilly, C. J. Hawker and K. L. Wooley, *Chem. Soc. Rev.*, 2006, **35**, 1068–1083.
3 J. Z. Du and R. K. O'Reilly, *Soft Matter*, 2009, **5**, 3544–3561.
4 W. Q. Chen and J. Z. Du, *Sci. Rep.*, 2013, **3**, DOI: 10.1038/srep02162.
5 A. Kumar, A. Srivastava, I. Y. Galaev and B. Mattiasson, *Prog. Polym. Sci*., 2007, **32**, 1205–1237.
6 A. K. Bajpai, S. K. Shukla, S. Bhanu and S. Kankane, *Prog. Polym. Sci*., 2008, **33**, 1088–1118.
7 D. Roy, J. N. Cambre and B. S. Sumerlin, *Prog. Polym. Sci*., 2010, **35**, 278–301.
8 H. Y. Tian, Z. H. Tang, X. L. Zhuang, X. S. Chen and X. B. Jing, *Prog. Polym. Sci*., 2012, **37**, 237–280.
9 W. Hua, R. X. Zhuo and X. Z. Zhang, *Prog. Polym. Sci*., 2013, **38**, 503–535.
10 S. Binauld and M. H. Stenzel, *Chem. Commun*., 2013, **49**, 2082−2102.
11 R. Cheng, F. H. Meng, C. Deng, H.-A. Klok and Z. Y. Zhong, *Biomaterials*, 2013, **34**, 3647−3657.
12 P. Schattling, F. D. Jochum and P. Theato, *Polym. Chem*., 2014, **5**, 25–36.
13 J. M. Zhuang, M. R. Gordon, J. Ventura, L. Y. Li and S. Thayumanavan, *Chem. Soc. Rev.,* 2013, **42**, 7421–7435.
14 Z. S. Ge and S. Y. Liu, *Chem. Soc. Rev*., 2013, **42**, 7289−7325.
15 R. Balu, J. Whittaker, N. K. Dutta, C. M. Elvin and N. R. Choudhury, *J. Mater. Chem. B*, 2014, **2**, 5936−5947.
16 A. Klaikherd, C. Nagamani and S. Thayumanavan, *J. Am. Chem. Soc.*, 2009, **131**, 4830–4838.
17 P. Schattling, F. D. Jochum and P. Theato, *Chem. Commun*., 2011, **47**, 8859–8861.

18 Z.-Y. Qiao, R. Zhang, F.-S. Du, D.-H. Liang and Z.-C. Li, *J. Control. Release*, 2011, **152**, 57−66.
19 P. Yang, D. Li, S. Jin, J. Ding, J. Guo, W. B. Shi and C. C. Wang, *Biomaterials*, 2014, **35**, 2079–2088.
20 S. Kumar, R. Acharya, U. Chatteriji and P. De, *J. Mater. Chem. B,* 2013, **1**, 946–957.
21 X. L. Hu, H. Li, S. Z. Luo, T. Liu, Y. Y. Jiang and S. Y. Liu, *Polym. Chem*., 2013, **4**, 695–706.
22 J. Xuan, D. H. Han, H. S. Xia and Y. Zhao, *Langmuir*, 2014, **30**, 410−417.
23 Y. Hao, J. L. He, S. Li, J. Liu, M. Z. Zhang and P. H. Ni, *J. Mater. Chem. B.* 2014, **2**, 4237-4249.
24 W. Shao, K. Miao, H. H. Liu, C. N. Ye, J. Z. Du and Y. L. Zhao, *Polym. Chem*., 2013, **4**, 3398–3410**.**
25 K. Miao, W. Shao, H. H. Liu and Y. L. Zhao, *Polym. Chem*., 2014, **5**, 1191**–**1201.
26 K. Miao, H. H. Liu and Y. L. Zhao, *Polym. Chem*., 2014, **5**, 3335–3345.
27 H. X. Huang, X. L. Jiang, Q. Z. Yang, Y. F. Chu, G. Y. Zhang, B. Yang and R. X. Zhuo, *J. Mater. Chem. B*, 2013, 1, 1860−1868.
28 S. J. Yu, C. L. He, J. X. Ding, Y. L. Cheng, W. T. Song, X. L. Zhuang and X. S. Chen, *Soft Matter*, 2013, **9**, 2637–2645.
29 S. Binauld, W. Scarano and M. H. Stenzel, *Macromolecules*, 2012, **45**, 6989–6999.
30 V. T. Huynh, S. Binauld, P. L. de Souza and M. H. Stenzel, *Chem. Mater*., 2012, **24**, 3197–3211.
31 Z.-Y. Qiao, R. Ji, X.-N. Huang, F.-S. Du, R. Zhang, D.-H. Liang and Z.-C. Li, *Biomacromolecules*, 2013, **14**, 1555−1563.
32 C. M. Jian, B-W. Liu, X. Chen, S-T. Liu, T. Fang, J. Y. Yuan, *Chinese J. Polym. Sci*., 2014, **32**, 690–702.
33 B. V. K. J. Schmidt, M. Hetzer, H. Ritter and C. Barner-Kowollik, *Macromolecules*, 2013, **46**, 1054−1065.
34 X. L. Hu, J. Tian, T. Liu, G. Y. Zhang and S. Y. Liu, *Macromolecules*, 2013, **46**, 6243−6256.
35 L. Ye, X. Q. Liu, K. Ito, Z. G. Feng, *J. Mater. Chem. B,* 2014, **2**, 5746−5757.
36 Q. M. Liu, S. Chen, J. Chen and J. Z. Du, *Macromolecules,* 2015, **48**, 739−749.
37 Y. Q. Zhu, F. Y. K. Wang, C. Zhang and J. Z. Du, *ACS Nano,* 2014, **8**, 6644−6654.
38 D. Klinger and K. Landfester, *Polymer*, 2012, **53**, 5209−5231.
39 J. Szejtli, *Chem. Rev*., 1998, **98**, 1743–1753.
40 M. E. Davis and M. E. Brewster, *Nat. Rev. Drug Discov*., 2004, **3**, 1023–1035.
41 K. Uekama, F. Hirayama and T. Irie, *Chem. Rev*., 1998, **98**, 2045–2076.
42 A. L. Laza-Knoerr, R. Gref and P. Couvreur, *J. Drug Target.*, 2010, **18**, 645–656.
43 J. W. Zhou and H. Ritter, *Polym. Chem*., 2010, **1**, 1552–1559.
44 J. X. Zhang and P. X. Ma, *Adv. Drug Deliver. Rev*., 2013, **65**, 1215–1233.
45 A. Concheiro and C. Alvarez-Lorenzo, *Adv. Drug Deliver. Rev.*, 2013, **65**, 1188–1203.
46 G. S. Chen and M. Jiang, *Chem. Soc. Rev.*, 2011, **40**, 2254–2266.
47 B. V. K. J. Schmidt, M. Hetzer, H. Ritter, C. Barner-Kowollik, *Macromol. Rapid Commun.,* 2013*,* **34***,* 1306−1311.
48 H. J. Zhang, Y. Xin, Q. Yan, L. L. Zhou, L. Peng and J. Y. Yuan, *Macromol. Rapid Commun.,* 2012*,* **33***,* 1952−1957.
49 J. Li, B. Chen, X. Wang and S. H. Goh, *Polymer*, 2004, **45**, 1777–1785.
50 A. Kulkarni, K. DeFrees, S.-H. Hyun and D. H. Thompson*, J. Am. Chem. Soc.*, 2012, **134**, 7596–7599.
51 G. Y. Liu, Q. Jin, X. S. Liu, L. P. Lv, C. J. Chen and J. Ji, *Soft Matter*, 2011, **7**, 662–669.
52 Y. Chen, Y. Pang, J. L. Wu, Y. Su, J. Y. Liu, R. B. Wang, B. S. Zhu, Y. F. Yao, D. Y. Yan, X. Y. Zhu and Q. Chen, *Langmuir*, 2010, **26**, 9011–9016.
53 F. Yhaya, S. Binauld, Y. Kim and M. H. Stenzel, *Macromol. Rapid Commun.,* 2012*,* **33***,* 1868−1874.
54 J. X. Zhang, K. Ellsworth and P. X. Ma, *Macromol. Rapid Commun.,* 2012*,* **33***,* 664−671.
55 A. Bertrand, M. Stenzel, E. Fleury and J. Bernard, *Polym. Chem*., 2012, **3**, 377–383.
56 F. Zhao, H. Yin, J. Li, *Biomaterials*, 2014, **35**, 1050–1062.
57 W. Y. Li, J. W. Du, K. Zheng, P. Zhang, Q. L. Hu and Y. X. Wang, *Chem. Commun.,* 2014, **50**, 1579–1581.
58 W. Zhu, Y. L. Li, L. X. Liu, Y. M. Chen and F. Xi, *Int. J. Pharm*., 2012, **437**, 11–19.
59 W. Zhu, Y. L. Li, L. X. Liu, Y. M. Chen, C. Wang and Fu Xi, *Biomacromolecules,* 2010**,** **11***,* 3086–3092.
60 H. Zou, W. Guo and W. Z. Yuan, *J. Mater. Chem. B*, 2013, **1**, 6235–6244.
61 X. F. Chen, L. Chen, X. M. Yao, Z. Zhang, C. L. He, J. P. Zhang and X. S. Chen, *Chem. Commun.,* 2014, **50**, 3789–3791.
62 S. S. Sheiko, B. S. Sumerlin and K. Matyjaszewski, *Prog. Polym. Sci.*, 2008, **33**, 759−785.
63 H.-i. Lee, J. Pietrasik, S. S. Sheiko and K. Matyjaszewski, *Prog. Polym. Sci*., 2010, **35**, 24−44.
64 C. Feng, Y. J. Li, D. Yang, J. H. Hu, X. H. Zhang and X. Y. Huang, *Chem. Soc. Rev*., 2011, **40**, 1282−1295.
65 H. F. Shi, Y. Zhao, X. Dong, Y. Zhou and D. J. Wang, *Chem. Soc. Rev*., 2013, **42**, 2075−2099.
66 M. M. Caruso, D. A. Davis, Q. Shen, S. A. Odom, N. R. Sottos, S. R. White and J. S. Moore, *Chem. Rev*., 2009, **109**, 5755–5798.
67 J. Z. Du, L. Y. Tang, W. J. Song, Y. Shi and J. Wang, *Biomacromolecules*, 2009, **10**, 2169–2174.
68 W. L. Zhang, Y. L. Li, L. X. Liu, Q. Q. Sun, X. T. Shuai, W. Zhu and Y. M. Chen, *Biomacromolecules*, 2010, **11**, 1331–1338.
69 X. M. Song, W. Q. Yao, G. L. Lu, Y. J. Li and X. Y. Huang, *Polym. Chem*., 2013, **4**, 2864–2875.
70 S. X. Li, C. N. Ye, G. D. Zhao, M. J. Zhang and Y. L. Zhao, *J. Polym. Sci., Part A: Polym. Chem*., 2012, **50**, 3135–3148.
71 Q. T. Huang, B. Yang, H. H. Liu, Y. L. Zhao and J. Z. Du, *Polym. Chem.,* 2015, **6**, 886–890.
72 M. J. Zhang, H. H. Liu, W. Shao, K. Miao and Y. L. Zhao, *Macromolecules*, 2013, **46**, 1325–1336.
73 J. Chiefari, Y. K. Chong, F. Ercole, J. Krstina, J. Jeffery, T. P. T. Le, R. T. A. Mayadunne, G. F. Meijs, C. L. Moad, G. Moad, E. Rizzardo and S. H. Thang, *Macromolecules*, 1998, **31**, 5559–5562.
74 Y. Mitsukami, M. S. Donovan, A. B. Lowe and C. L. McCormick, *Macromolecules*, 2001, **34**, 2248–2256.
75 D. J. Pochan, Z. Y. Chen, H. G. Cui, K. Hales, K. Qi and K. L. Wooley, *Science*, 2004, **306**, 94–97.
76 Z. Y. Chen, H. G. Cui, K. Hales, Z. B. Li, K. Qi, D. J. Pochan and K. L. Wooley, *J. Am. Chem. Soc*., 2005, **127**, 8592–8593.
77 H. G. Cui, Z. Y. Chen, K. L. Wooley and D. J. Pochan, *Soft Matter*, 2009, **5**, 1269–1278.
78 L. Chen, T. Jiang, J. P. Lin and C. H. Cai, *Langmuir*, 2013, **29**, 8417–8426.
79 J.-K. Kim, E. Lee, Z. Huang and M. Lee, *J. Am. Chem. Soc.,* 2006, **128**, 14022−14023.
80 E. Lee, Y.-H. Jeong, J.-K. Kim and M. Lee, *Macromolecules,* 2007, **40***,* 8355–8360.
81 C.-Y. Hsu, S.-C. Chang, K.-Y. Hsu and Y.-L. Liu, *Macromol. Rapid Commun.,* 2013*,* **34***,* 689–694.
82 Y. Q. Zhu, L. Liu and J. Z. Du, *Macromolecules*, 2013, **46**, 194–203.

 

Graphical Abstract:

# Multi-responsive graft copolymer micelles comprising acetal and disulfide linkages for stimuli-triggered drug delivery

Huanhuan Liu, Cangxia Li, Dandan Tang, Xiaonan An, Yanfei Guo and Youliang Zhao

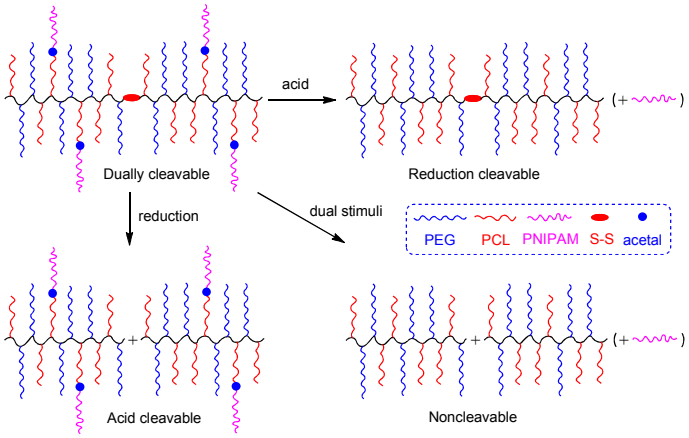


Dual-cleavable polymeric aggregates were efficiently used for thermo, pH and reduction triggered controlled release of doxorubicin due to stimuli-dependent topological transformation and reaggregation of copolymer aggregates.